# Finite-Difference Solution for Three-Dimensional Boundary Layers with Large Positive and Negative Crossflows

ANASTASIUS J. KARABELAS* AND THOMAS J. HANRATTY†
*Department of Chemical Engineering, University of Illinois, Urbana, Ill.*

**This paper shows how finite-difference methods can be used to analyze three-dimensional boundary layers on axisymmetric bodies with large positive and negative crossflows. The particular problem considered is the flow around a sphere in a single layer of spheres. The external flow is given by the potential solution and is obtained by doing experiments in an electrolytic tank. The computational scheme was found to be stable provided that the components of the wall velocity gradient along the meridians were positive. The solution covered regions of both positive and negative crossflows so that the angle between the limiting steamlines and the meridians varied between +33° and −90°. These computational results are consistent with an analysis of the stability of the numerical scheme.**

## I. Introduction

FINITE-DIFFERENCE methods are now widely used to solve the equations for two-dimensional boundary layers. This paper shows how such techniques can be applied to an axisymmetric body having a three-dimensional boundary layer with large positive and negative crossflows.

We consider the laminar boundary layer on a sphere in a single layer of spheres for which the external flow is given by potential theory. Because of the very large crossflows, particular attention had to be paid to the stability of the calculations. The computational scheme developed is also of interest in that the external flow was determined from experiments in an electrolytic tank and therefore is given in tabular form. Boundary-layer separation can cause the flow external to the boundary layer to be different from that predicted by potential theory. Therefore the calculated results can be expected to disagree with measurements, particularly near separation.

The two methods that have been most widely used for three-dimensional boundary layers involve series expansions or integral forms of the momentum equations. (Series solutions have been reviewed by Crabtree, Küchemann, and Sowerby.[1]) They are limited in that they are conveniently applied only in a region close to the birthplace of the boundary layer. Momentum integral methods have usually been formulated in an "intrinsic" system of coordinates constructed from the projections of the external streamlines and their orthogonals. They have been most useful when a "small crossflow approximation" can be made whereby the velocity components in the boundary layer perpendicular to the direction of the external streamlines can be assumed to be small. A review of this category of solutions is given by Cooke and Hall.[2] Integral methods are not conveniently applied to the problem considered in this paper because equations for an intrinsic set of coordinates are not easily derived and because a small crossflow approximation would not be applicable.

Very recently Der and Raetz,[3] Hall,[4] and Dwyer[5] applied finite-difference methods to three-dimensional boundary layers. The difference approximations used are implicit in the direction normal to the solid surface and explicit in the tangential directions. The results of Hall and Dwyer are encouraging with respect to the possibility of developing stable and efficient computational methods. However, the numerical schemes proposed by them do not yield a stable solution to the problem being considered. It was therefore necessary for us to clarify the effect of negative and positive crossflows on stability. We present a numerical scheme which, from a recent analysis by Krause, Hirschel, and Bothmann[6] appears to be the most stable one for finite difference approximations that are explicit in the tangential directions.

## II. Definition of the Problem

The flow problem considered in this paper is sketched in Fig. 1. Each sphere is in contact with four others at points $C_1$, $C_2$, $C_3$, and $C_4$. Consider the system of coordinates shown in Fig. 2. At $\phi = 0°$, there is a frontal point of attachment. The contact points are located at $\phi = 90°$ and $\theta = 0°$, 90°, 180°, and 270°. The four major circles at $\theta = 0°$, 45°, 90°, and 135° divide the spherical surface into eight identical segments.

It is necessary only to examine the flowfield bounded by the solid surface and the two planes formed by the normals to the surface along $\theta = 0°$ and $\theta = 45°$. These planes and the lines $S_1$ and $S_2$ will be called planes of symmetry and meridians of symmetry.

A system of boundary-layer coordinates $(x, y, z)$ has been chosen such that the lines $y$ = constant represent the meridians on the surface of the sphere and the lines $x$ = constant, trajectories perpendicular to the meridians. The coordinate

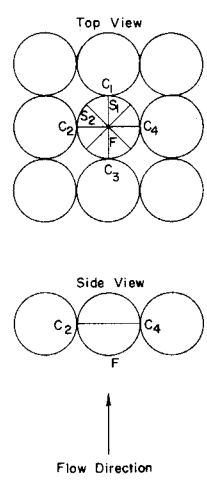


**Fig. 1 Orientation of single layer of spheres.**

Received August 6, 1970; revision received January 4, 1971. This work has been partially supported by the National Science Foundation under Grant NSF GK-2813.

Index Category: Boundary Layers and Convective Heat Transfer—Laminar.

* Research Fellow, presently with Shell Pipeline Research, Houston, Texas.

† Professor of Chemical Engineering.

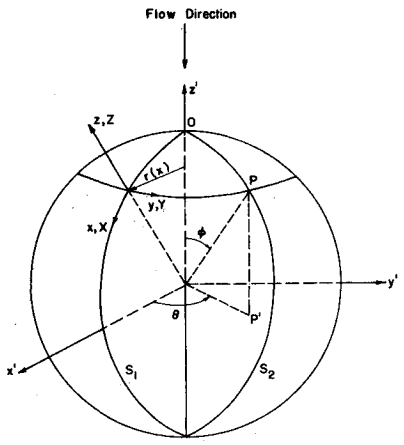


**Fig. 2 System of coordinates.**

$z$ is measured along lines normal to the surface. The velocity components tangent to the $x$, $y$, and $z$ coordinates are respectively $u$, $v$, and $w$. An element of length, $dl$, is given as

$$dl^2 = h_x^2(dx^2) + h_y^2(dy)^2 + (dz)^2 \tag{1}$$

with metric coefficients $h_x = 1$ and $h_y = r(x)$, where $r(x)$ is defined in Fig. 2 and is given as

$$r(x) = R \sin(x/R) \tag{2}$$

and $R$ is the radius of the sphere.

The variables of the problem are made dimensionless in the following way

$$X = x/R \quad Y = y \quad Z = z/R(Re/2)^{1/2} \quad r^* = r/R$$

$$U = u/U_\infty \quad V = v/U_\infty \quad W = w/U_\infty(\mathrm{Re}/2)^{1/2}$$

$$P = (p/\tfrac{1}{2}\rho U_\infty^2) \tag{3}$$

Here $Re$ is the Reynolds number, $U_\infty$, the velocity of the fluid approaching the layer, and $p$, the pressure. The dimensionless velocity gradients at the wall are $S_x$ and $S_y$ and the angle of deviation, $\alpha_w$, of the wall stress with reference to the positive x-direction is defined as $\alpha_w = \arctan(S_y/S_x)$.

The boundary-layer equations are given as

$$U\frac{\partial U}{\partial X} + \frac{V}{\sin X}\frac{\partial U}{\partial Y} + W\frac{\partial U}{\partial Z} - V^2\cot X = -\frac{1}{2}\frac{\partial P}{\partial X} + \frac{\partial^2 U}{\partial Z^2} \tag{4}$$

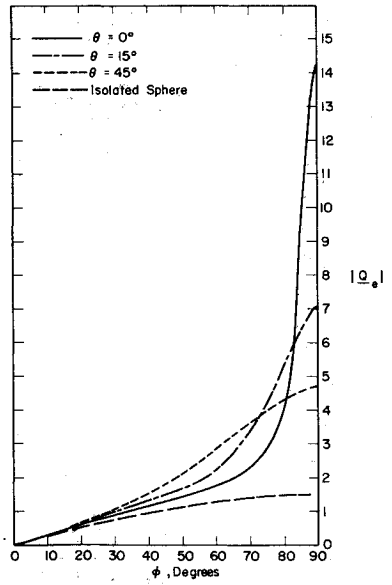


**Fig. 3 Potential flow, velocity variation along various meridians.**

$$U\frac{\partial V}{\partial X} + \frac{V}{\sin X}\frac{\partial V}{\partial Y} + W\frac{\partial V}{\partial Z} + UV\cot X = -\frac{1}{2\sin X}\frac{\partial P}{\partial Y} + \frac{\partial^2 V}{\partial Z^2} \tag{5}$$

$$U\cot X + \frac{\partial U}{\partial X} + \frac{1}{\sin X}\frac{\partial V}{\partial Y} + \frac{\partial W}{\partial Z} = 0 \tag{6}$$

The boundary conditions on $Z$ are $U = V = W = 0$ at $Z = 0$ and $U = U_e$, $V = V_e$ as $Z \to \infty$. The velocity components, $U_e$ and $V_e$, external to the boundary layer are defined by potential flow theory and the derivatives of the pressure are given by the Euler equations evaluated at the surface.

## III. The External Flowfield

It was not apparent how to obtain an analytic solution to the Laplace equation for the geometry considered in this problem. Therefore an electrolytic tank[7] was used to determine $U_e$ and $V_e$. The tank contained a solution of conducting fluid and two opposite walls were electrodes. A layer of spheres was immersed in the fluid in the tank with its plane parallel to the electrodes. A voltage difference was maintained between the electrodes. The velocities $U_e$ and $V_e$ calculated from measurements of the potential gradients at different locations on the surface of one of the spheres in the layer are believed to be accurate within $\pm 5\%$ except near a contact point. Details regarding these measurements are contained in a thesis by one of the authors.[8]

Some of the results from these measurements are shown in Figs. 3 and 4. The vector $\mathbf{Q_e}$ plotted in these figures is tangent to the surface of the sphere and has components $U_e$ and $V_e$. The angle which the vector $\mathbf{Q_e}$ makes with the $X$ axis is designated as $\alpha_e$ and is defined as

$$\alpha_e = \arctan(V_e/U_e) \tag{7}$$

Results are presented only for the front part of the sphere ($\phi = 0°$–$90°$) since the potential field is symmetric with respect to the equatorial plane ($\phi = 90°$).

As can be seen in Fig. 3 the velocity $\mathbf{Q_e}$ changes dramatically along the meridians. Extremely high velocities were measured in the vicinity of the contact point. The velocity is approximately axisymmetric up to $\phi = 10°$ and from $\phi = 0°$ to $\phi = 5°$ it agrees with what would be determined for an isolated sphere; i.e.,

$$U_e = (3/2)U_\infty \sin X \tag{8}$$

Farther downstream the influence of neighboring spheres causes large lateral gradients in the velocity. Up to $\phi = 90°$ the velocity increases with increasing $\phi$.

Figure 4 shows the variation of the angle $\alpha_e$ along various meridians. The largest deviations of $\mathbf{Q_e}$ from the $X$ coordinate occur close to the meridians which pass through contact points.

## IV. Finite-Difference Scheme

The finite-difference scheme used to solve Eqs. (4–6) is explicit in the $X$ and $Y$ directions and implicit in the $Z$ direction. First-order derivatives in the $X$ and $Z$ directions were approximated by central differences and second-order derivatives by the Crank-Nicholson 6-point formula. A "mixed" formula involving the average of a forward and a backward difference approximation was employed for derivatives in the $Y$ direction. This difference representation was found to be essential for the stability of the over-all computational scheme, as will be explained later. In fact, the stability of a scheme based on a central difference approximation of the $Y$-derivatives, such as that used by Dwyer,[5] was proven to be unsatisfactory. Figure 5 shows the three-dimensional grid used throughout the computations.

Suppose that the initial conditions along the normals $(r,s)$, $(r,s-1)$, $(r,s-2)$, etc. and the boundary conditions (on the plane $S_2$ in Fig. 5) along the normals $(r,s)$, $(r+1,s)$, $(r+2,s)$, etc. are known. Then we can make the following approximations at a point $C$ with indices $(r+\frac{1}{2}, s-1, t)$:

$$\partial F/\partial X = (F_{r+1,s-1}{}^{t} - F_{r,s-1}{}^{t})/\Delta X \tag{9}$$

$$\partial F/\partial Y = (F_{r+1,s}{}^{t} - F_{r+1,s-1}{}^{t} + F_{r,s-1}{}^{t} - F_{r,s-2}{}^{t})/2\Delta Y \tag{10}$$

$$\partial F/\partial Z = (F_{r+1,s-1}{}^{t+1} - F_{r+1,s-1}{}^{t-1} + F_{r,s-1}{}^{t+1} - F_{r,s-1}{}^{t-1})/4\Delta Z \tag{11}$$

$$\partial^2 F/\partial Z^2 = (F_{r+1,s-1}{}^{t+1} - 2F_{r+1,s-1}{}^{t} + F_{r+1,s-1}{}^{t-1})/2\Delta Z^2 + (F_{r,s-1}{}^{t+1} - 2F_{r,s-1}{}^{t} + F_{r,s-1}{}^{t-1})/2\Delta Z^2 \tag{12}$$

where $F$ designates a dependent variable. Upon substituting Eqs. (9–12) into Eq. (4) and rearranging we obtain

$$\begin{aligned} &U_{r+1,s-1}{}^{t-1}\left[-\frac{(W)_c}{4\Delta Z} - \frac{1}{2\Delta Z^2}\right] + U_{r+1,s-1}{}^{t} \times \left[\frac{(U)_c}{\Delta X} - \frac{1}{2\Delta Y}\left(\frac{V}{\sin X}\right)_c + \frac{1}{\Delta Z^2}\right] + U_{r+1,s-1}{}^{t+1} \times \left[\frac{(W)_c}{4\Delta Z} - \frac{1}{2\Delta Z^2}\right] = U_{r,s-1}{}^{t-1}\left[\frac{(W)_c}{4\Delta Z} + \frac{1}{2\Delta Z^2}\right] + \\ &U_{r,s-1}{}^{t}\left[\frac{(U)_c}{\Delta X} - \frac{1}{2\Delta Y}\left(\frac{V}{\sin X}\right)_c - \frac{1}{\Delta Z^2}\right] + U_{r,s-1}{}^{t+1} \times \left[-\frac{(W)_c}{4\Delta Z} + \frac{1}{2\Delta Z^2}\right] - (U_{r+1,s}{}^{t} - U_{r,s-2}{}^{t}) \times \left[\frac{1}{2\Delta Y}\left(\frac{V}{\sin X}\right)_c\right] + (V^2 \cot X)_c + \left(-\frac{1}{2}\frac{\partial P}{\partial X}\right)_c \end{aligned} \tag{13}$$

where the subscript $c$ indicates conditions at the center point $C(r+\frac{1}{2}, s-1, t)$. In order to linearize Eq. (13) the velocities at $C$ are approximated by the backward difference formula

$$(F)_c = (3F_{r,s-1}{}^{t} - F_{r-1,s-1}{}^{t})/2 \tag{14}$$

The pressure derivative is calculated from tabulated values of $U_e$ and $V_e$ using the Euler equations. An equation similar to Eq. (13) can be obtained from the $Y$-momentum equation, Eq. (5). The only difference is in the term $UV \cot X$ which is approximated as follows

$$(UV \cot X)_c = (U \cot X)_c[(V_{r+1,s-1}{}^{t} + V_{r,s-1}{}^{t})/2] \tag{15}$$

It will be noticed that difference equations, such as Eq. (13) are linear, uncoupled and contain unknown quantities at three points along the normal $(r+1, s-1)$. Successive application of Eq. (13) from the surface $(Z=0)$, at which $U_{r+1,s-1}{}^{t-1} = 0$, up to the edge of the boundary layer $(Z \to \infty)$, at which $U_{r+1,s-1}{}^{t+1} = (U_e)_{r+1,s-1}$, results in a system of linear algebraic equations. The corresponding matrix of coefficients is of tridiagonal form and the system can be solved by an efficient algorithm due to Thomas.[9] In this fashion the velocity components $U$ and $V$ are calculated along the normal $(r+1, s-1)$.

The $W$ velocity component is calculated from the continuity equation, Eq. (6). The following central-difference approximations are made in this case

$$\frac{\partial U}{\partial X} = (U_{r+1,s-1}{}^{t} - U_{r,s-1}{}^{t} + U_{r+1,s-1}{}^{t-1} - U_{r,s-1}{}^{t-1})/2\Delta X \tag{16}$$

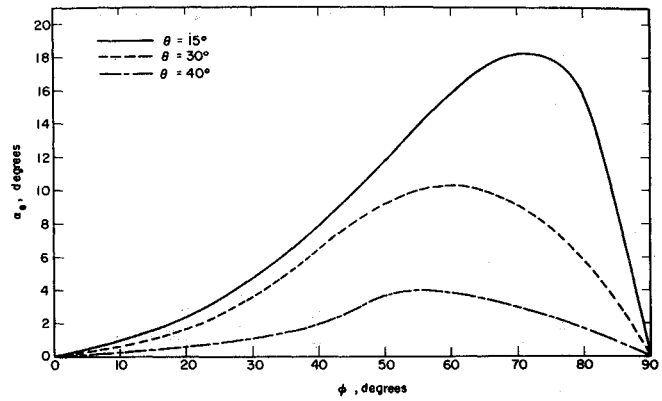


**Fig. 4 Variation of angle of deviation, $\alpha$, along various meridians.**

$$\frac{\partial V}{\partial Y} = (V_{r+1,s}{}^{t} - V_{r+1,s-1}{}^{t} + V_{r,s-1}{}^{t} - V_{r,s-2}{}^{t})/4\Delta Y + (V_{r+1,s}{}^{t-1} - V_{r+1,s-1}{}^{t-1} + V_{r,s-1}{}^{t-1} - V_{r,s-2}{}^{t-1})/4\Delta Y \tag{17}$$

$$\frac{\partial W}{\partial Z} = (W_{r+1,s-1}{}^{t} - W_{r+1,s-1}{}^{t-1} + W_{r,s-1}{}^{t} - W_{r,s-1}{}^{t-1})/2\Delta Z \tag{18}$$

$$U_{r+1/2,s-1/2}{}^{t-1/2} = (U_{r+1,s-1}{}^{t} + U_{r+1,s-1}{}^{t-1} + U_{r,s-1}{}^{t} + U_{r,s-1}{}^{t-1})/4 \tag{19}$$

Substitution of Eqs. (16–19) into Eq. (6) yields an expression for the velocity component $W_{r+1,s-1}{}^{t}$. Starting the computations at the surface, so that $W_{r+1,s-1}{}^{t-1} = 0$ (boundary condition at $Z = 0$), and advancing upwards the velocities $W_{r+1,s-1}{}^{t}$, $W_{r+1,s-1}{}^{t+1}$, $W_{r+1,s-1}{}^{t+2}$, etc. are calculated consecutively. The $W$ velocities are computed, of course, after $U$ and $V$ have been evaluated all along the normal $(r+1, s-1)$.

## V. Conditions on the Initial Plane and on the Plane of Symmetry

The computational scheme outlined in the previous section requires that values of $U$ and $V$ be specified on some plane $X_i$ = constant and on one of the planes of symmetry.

Since the external flow is axisymmetric for small values of $X$, accurate initial conditions can be established by using results of the series solution due to Frössling[10] with $U_e$ given by Eq. (8). A truncation of terms involving powers larger than 5 provides sufficient accuracy at a distance $X = 0.03$ ($\phi \simeq 2°$). This station was selected for tabulating initial conditions.

It is possible to use either the plane of symmetry at $Y = \pi/4$ (corresponding to meridian $S_2$ in Fig. 2) or at $Y = 0$ (meridian $S_1$) as a boundary plane for the calculations. The meridian $S_2$ was chosen for three reasons. First $S_1$ passes through a contact point at which the accuracies of the

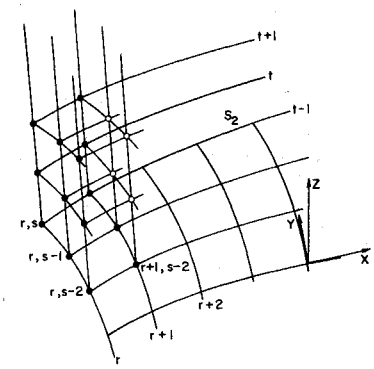


**Fig. 5 Grid for the finite-different scheme.**

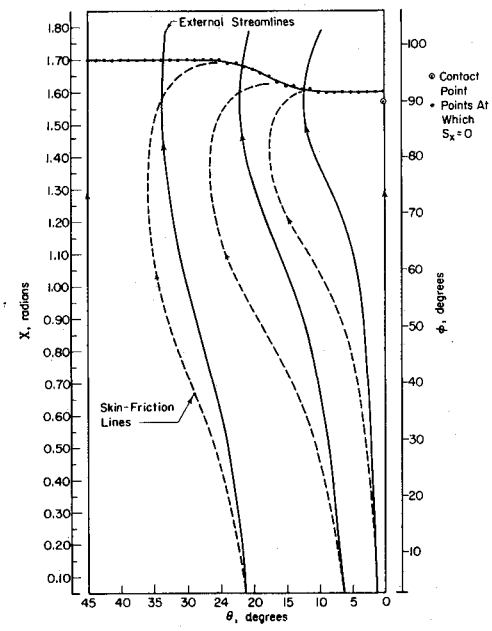


**Fig. 6 Flow development based on potential external field.**

measured $U_e$ and $V_e$ and of the calculations are questionable. If the calculations start at $S_2$ it is possible to terminate them a few steps away from $S_1$ in the neighborhood of the contact point. Second the tabulated values of $U_e$ and $V_e$ are smoother near $S_2$ and it is therefore possible to determine lateral derivatives more accurately. Third it was computationally convenient because flow separation occurs earlier along $S_1$ than along $S_2$. As suggested by Dwyer[11] the uniqueness of the solution was checked up to about $X = 0.50$ ($\phi \cong 30°$) by showing that results of calculations starting from $Y = 0$ and $Y = \pi/4$ are indistinguishable. An additional check on the reliability of the calculations (using $Y = \pi/4$ as the starting meridian) was obtained by calculating $V$ on $Y = 0$ for each $X$-station. The difference from the known boundary condition, $V = 0$, was always of the order of the single-precision arithmetic error of the computer ($\sim 10^6$).

On the symmetry plane the velocity component $V$ is zero. The velocity component $U$ is defined by the following form of the $X$-momentum equation

$$U(\partial U/\partial X) + W(\partial U/\partial Z) = -\tfrac{1}{2}(\partial P/\partial X) + \partial^2 U/\partial Z^2 \quad (20)$$

The velocity component $W$ in this equation is evaluated from the equation of conservation of mass, Eq. (6). It is seen that in order to solve Eq. (6) values of $\partial V/\partial Y = V_Y$ should be known along the symmetry plane.

Moore[12] and Dwyer[5] have suggested the differentiation of the $Y$-momentum equation and the treatment of $V_Y$ as a

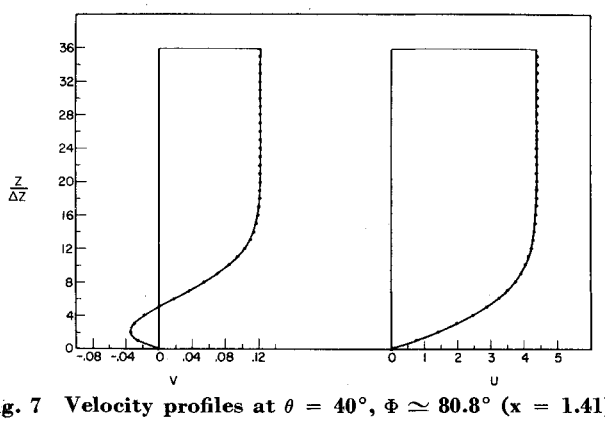


**Fig. 7 Velocity profiles at $\theta = 40°$, $\Phi \simeq 80.8°$ ($x = 1.41$).**

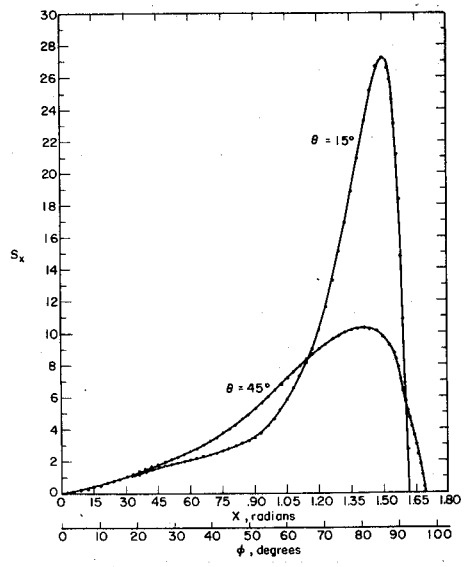


**Fig. 8 Variation of $S_x$ along two meridians.**

dependent variable on the symmetry plane. From Eq. (5)

$$U\frac{\partial V_Y}{\partial X} + \frac{V_Y^2}{\sin X} + W\frac{\partial V_Y}{\partial Z} + UV_Y \cot X = -\frac{1}{2\sin X}\frac{\partial^2 P}{\partial Y^2} + \frac{\partial^2 V_Y}{\partial Z^2} \quad (21)$$

It is seen that the solution of this equation requires accurate information on the pressure or on the external flow near the line of symmetry. An alternate procedure for evaluating $V_Y$ could involve a backward interpolation of the values of $V$ calculated by the finite difference scheme outlined in the previous section. It was found that the measurements from the electrolytic tank were precise enough near $S_2$ that the direct approach of Moore could be used.

Values of $U$ along $S_2$ were calculated from Eqs. (20, 21, and 6) using the boundary conditions $U = V_Y = 0$ at $Z = 0$ and $U = U_e, V = V_e$ at $Z \to \infty$. The finite difference representations of these equations are based on formulas (9, 11, 12, and 14). The term $UV_Y \cot X$ in Eq. (21) is approximated by an expression similar to Eq. (15) and the term $V_Y^2/\sin X$ is replaced by $[(V_Y)_{r+1,s}{}^t] \cdot [(V_Y)_{r,s}{}^t]/\sin X$ in order to obtain a first order algebraic equation for the unknown $(V_Y)_{r+1,s}{}^t$. The equation of continuity on the symmetry plane is solved

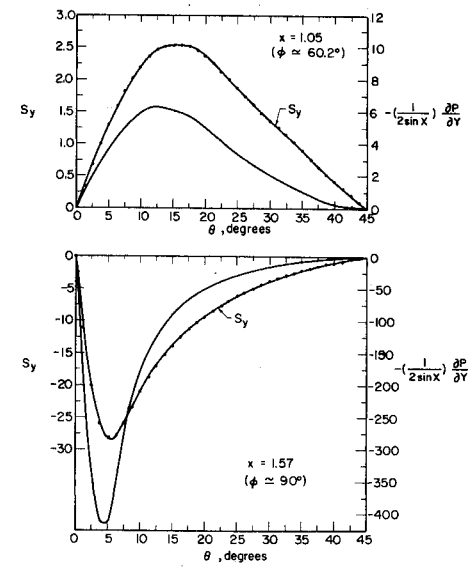


**Fig. 9 Variation of $S_y$ and $-(1/2 \sin X)(\partial P/\partial Y)$ in the lateral direction.**

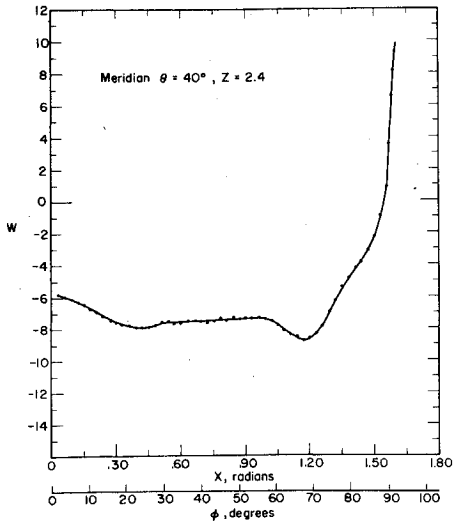


FIG. 10 NORMAL VELOCITY DISTRIBUTION CLOSE TO THE EDGE OF THE BOUNDARY LAYER

**Fig. 10 Normal velocity distribution close to the edge of the boundary layer.**

in the same fashion as for the rest of the flowfield. In the case of the symmetry plane, however, the term $(\partial V/\partial Y)$, which is treated as a dependent variable, is approximated by the formula (19).

## VI. Stability of the Numerical Scheme

The stability of the numerical scheme will be examined by using the von Neumann method discussed in the book by Richtmyer and Morton.[13] The results are consistent with a recent analysis by Krause, Hirschel, and Bothmann[6] that is not exact as it is based on a linearized form of the difference equations. However, Richtmyer and Morton[13] emphasize that experience has shown the reliability of practical stability criteria obtained from this type of analysis.

The $X$-momentum equation is written in the following inearized form:

$$\frac{U}{\Delta X}[U_{r+1,s-1}{}^{t} - U_{r,s-1}{}^{t}] + \frac{V}{2\sin X \Delta Y} \times [U_{r+1,s}{}^{t} - U_{r+1,s-1}{}^{t} + U_{r,s-1}{}^{t} - U_{r,s-2}{}^{t}] - \frac{1}{2\Delta Z^2}[U_{r+1,s-1}{}^{t+1} - 2U_{r+1,s-1}{}^{t} + U_{r+1,s-1}{}^{t-1}] - \frac{2}{2\Delta Z^2}[U_{r,s-1}{}^{t+1} - 2U_{r,s-1}{}^{t} + U_{r,s-1}{}^{t-1}] = \left[V^2 \cot X - W\frac{\partial V}{\partial Z} - \frac{1}{2}\frac{\partial P}{\partial X}\right]^{t}_{r+1/2,s-1} \quad (22)$$

where the coefficients of the convective terms and terms containing lower order derivatives of $Z$ are taken as constants.

The amplification matrix, $G(\Delta x)$, for this equation has a single element and only one eigenvalue $\lambda$ so that

$$G(\Delta x) = \frac{2 + H - 2\alpha' \sin^2\beta' - i\alpha' \sin 2\beta'}{2 - H - 2\alpha' \sin^2\beta' + i\alpha' \sin 2\beta'} = \lambda \quad (23)$$

where $\alpha' = V\Delta X/U(\sin X)\Delta Y$, $H = -2\Delta X/U\Delta Z^2(1 - \cos l\Delta Z)$, $\beta' = k\Delta Y/2$, and $k$, $l$ are real numbers. The von Neumann condition for stability $|\lambda| \leq 1$ gives the relation

$$\frac{\{4[(1 - \alpha' \sin^2\beta') + H/2]^2 + (\alpha' \sin 2\beta')^2\}^{1/2}}{\{4[(1 - \alpha' \sin^2\beta') - H/2] + (\alpha' \sin 2\beta')^2\}^{1/2}} \leq 1 \quad (24)$$

which must hold for all real $k$ and $l$. For positive $U$ and $\Delta X$, $H \leq 0$ and $H = 0$ for $\cos l\Delta Z = 1$. The inequality (24) is satisfied for $(1 - \alpha' \sin^2\beta') \geq 0$. It follows that $-\infty \leq \alpha' \leq 1$ since the bound on the amplification factor must hold for all values of $k$. Therefore, the criterion for stability is

$$-\infty \leq (1/\sin X)(V/U)(\Delta X/\Delta Y) \leq 1 \quad (25)$$

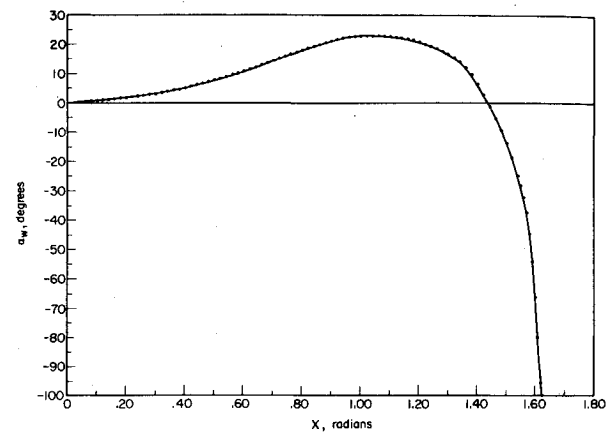


**Fig. 11 Variation of angle of deviation, $\alpha_w$, along the meridian $\theta = 15°$.**

The above relation indicated that the computational scheme is stable for negative lateral velocities, $V$, of any magnitude as long as the streamwise velocity component, $U$, remains positive. This property is of special importance in the calculation of three-dimensional boundary layers in which a large velocity divergence, without flow detachment, can occur. The region of stability with respect to the $X$-coordinate can be determined from the relationship (25). Suppose, for the moment, that $\Delta X = \Delta Y$ and $\sin X = 1$ (at the equator of the sphere). Then the scheme is stable for $-90° \leq \alpha \leq 45°$, i.e., the region of stability is 135°. The relationship (25) suggests that for a constant step-size ratio, $\Delta X/\Delta Y$, the region of stability is a function of $X$ due to the factor $1/\sin X$. However, with the proper choice of $\Delta X/\Delta Y$ (approximately 0.46 in our computations) the effect of $\sin X$, which might be troublesome in the front of the sphere or downstream of the equator, can be substantially reduced.

The numerical results presented in this paper support these conclusions regarding the stability of the scheme. Other methods of making the finite difference approximations would yield different stability criteria. The recent paper by Krause, Hirschel, and Bothmann[6] would suggest that the scheme employed in this paper is the best with regard to the size of the region of stability.

## VII. Problem Parameters

The finite-difference calculations were started at $X = 0.030$ ($\phi \simeq 1.7°$). A streamwise step $\Delta X = 0.010$ was sufficiently small to prevent any thickening of the boundary layer due to numerical errors. Calculations with $\Delta X = 0.005$ and 0.015 did not differ appreciably. However, step sizes $\Delta X > 0.015$ resulted in oscillations in the streamwise variation of the normal velocity component. A lateral step size $\Delta Y = 0.02182$ ($\Delta\theta = 1.25°$) gave a ratio $\Delta X/\Delta Y \simeq 0.458$, which was suitable from the standpoint of our analysis of the stability of the computational scheme. The step size in the normal direction was $\Delta Z = 0.075$ and the computations started with thirty-five steps of equal size. Tests with step sizes of 0.050 and 0.100 gave the same results and $\Delta Z = 0.075$ was selected because it provides satisfactory accuracy in the computation of the velocity gradient. The thickening of the boundary layer was taken into account by comparing $U_e = U_{r+1,s-1}{}^{t+1}$ and the last computed value $U_{r+1,s-1}{}^{t}$. If the difference was larger than a small prescribed constant (usually $10^{-4}$), the number of steps was increased by one and the profile recalculated.

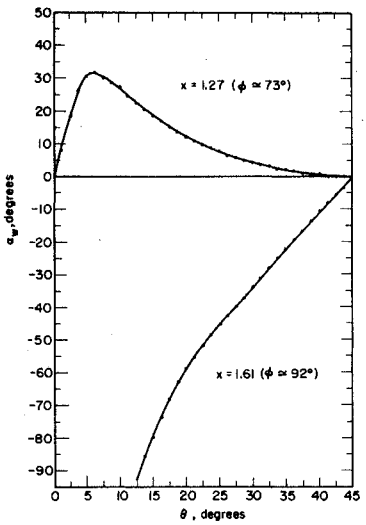


**Fig. 12 Variation of angle of deviation, $\alpha_w$, in the lateral direction.**

The line at which $S_x$ changes sign was determined. Beyond this line the computations were unstable. The gradient $S_x$ became negative first at a point close to $Y = 0$ ($\theta = 0°$). This point was excluded from the set of initial conditions for the next series of computations and the number of steps in the lateral direction was reduced. The same procedure was applied to other points until the computations covered the entire region of forward flow; i.e., until a negative $S_x$ was computed on the meridian $\theta = 45°$.

The computer programs, written in the FORTRAN IV language, occupied approximately 250 kilobytes of the computational memory. The computations were performed on the University of Illinois IBM Computer, Model 360/75. The total time required by the 360/75 processor for a complete solution was less than five min. The complete solution involved the calculation of $U$, $V$ and $W$ velocities at about 270,000 grid points in the space (for a maximum value of $X = 1.71$). The wall gradients, $S_x$ and $S_y$, the angle of derivation, $\alpha_w$, and the coordinates of the skin-friction lines at 6800 points were also computed.

## VIII. Results

The limiting streamlines close to the surface and the streamlines of the external flow are plotted in Fig. 6. These were obtained by solving the differential equation

$$dY/dX = (1/\sin X)(S_y/S_x) = 1/\sin X \tan\alpha_w$$

or (26)

$$dY/dX = (1/\sin X)(V_e/U_e) = 1/\sin X \tan\alpha_e$$

numerically using the "modified Euler's method."[9] The dots in Fig. 6 represent the points at which $S_x = 0$. At $\theta = 45°$, $S_x = 0$ at $\phi = 97.4°$. The line $S_x = 0$ seems to correspond roughly to an envelope for the limiting streamlines.

Typical velocity profiles are shown in Fig. 7. For this particular location the velocity component $V$ has a different sign close to the surface than at the edge of the boundary layer. Computed values of $S_x$ and $S_y$ are shown in Figs. 8 and 9. It is seen that the crossflow velocities assume rather large values. The large streamwise pressure gradients indicated by Fig. 3 cause a peak in $S_x$ close to the contact point. The strong influence of the lateral pressure gradients on the crossflow is evidence by the comparison of $S_y$ with $-(\frac{1}{2}\sin X)\cdot\partial P/\partial Y$ in Fig. 9. Of particular interest is the profile for the equator for which $V_e = 0$. The $W$ velocity component was found to be very sensitive to inaccuracies in the boundary conditions or to oscillations due to round-off errors. Values of $W$ close to the edge of the boundary layer are plotted in Fig. 10. Very large positive values of $W$ are obtained in the region where $S_x$ decreases from its maximum value to zero.

Values of $\alpha_w$ shown in Figs. 11 and 12 are consistent with the analysis of the stability of the numerical scheme. Figure 11 shows that the scheme has been tested in a region between $\alpha_w = +23°$ and $\alpha_w = -95°$. Figure 12 shows the scheme to be stable over a range of $\alpha$'s of 122°. The largest value of $\alpha_w$ found was +33°.

## IX. Discussion

The chief contribution of this paper is the demonstration of a stable scheme for calculating three-dimensional boundary layers for which $\alpha_w$ varies from +33° to −90°. These results are consistent with our analyses of the stability of the scheme.

The measured pressure variation over the surface of the sphere[8] agrees approximately with that calculated from the potential theory up to $\phi = 60°$. This suggests that the solution presented would not correspond to test results for $\phi > 60°$. This is clearly indicated by visual studies[8] which show that a saddle point rather than a nodal point, exists in the neighborhood of the contact point.

An attempt is now being made to carry out the numerical calculations using directly measured pressure variations over the surface of the sphere. Some difficulties are being encountered because of the requirement of highly accurate pressure measurements and because of the need to develop numerical schemes to relate the external velocity field to the measured pressures.

## References

[1] Crabtree, L. F., Küchemann, D., and Sowerby, L., "Three-Dimensional Boundary Layers," *Laminar Boundary Layers*, Pt. 8, edited by L. Rosenhead, Clarendon, Oxford, 1963.

[2] Cooke, J. C. and Hall, M. G., "Boundary Layers in Three Dimensions," *Progress in Aeronautical Sciences*, Vol. 2, Macmillan, New York, 1962.

[3] Hall, M. G., "A Numerical Method for Calculating Three-Dimensional Laminar Boundary Layers," TR 67145, 1967, Royal Aircraft Establishment.

[4] Der, J., Jr. and Raetz, G. S., "Solution of General Three-Dimensional Laminar Boundary Layer Problems by an Exact Numerical Method," Paper 62-70, Jan. 1962, IAS.

[5] Dwyer, H. A., "Solution of a Three-Dimensional Boundary-Layer Flow with Separation," *AIAA Journal*, Vol. 6, No. 7, 1968, pp. 1336–1342.

[6] Krause, E., Hirschel, E. H., and Bothmann, T., "Numerische Stabilität dreidimensionaler Grenzschichtlösungen," *Zetishrift für Angewandte Mathematik und Mechanik*, Sorderheft 48, No. 8, 1968, pp. T205–T208.

[7] Vitkovitch, D., *Field Analysis*, Van Nostrand, London, 1966.

[8] Karabelas, A. J., "Flow Through Regular Assemblies of Spheres," Ph.D. thesis, 1970, Univ. of Illinois, Urbana, Ill.

[9] Lapidus, L., *Digital Computation for Chemical Engineers*, McGraw-Hill, New York, 1962.

[10] Frössling, N., "Verdunstung, Wärmeübergang und Geschwindigketisverteilung bei zewidimensionaler und rotationssymmetrischer laminarer Grezschichtströmung," translated as TM 1432, NACA.

[11] McCroskey, W. J. and Dwyer, H. A., *Methods of Analyzing Propellor and Rotary Boundary Layers with Crossflow*, NASA SP-228, Oct. 1969.

[12] Moore, F. K., "Laminar Boundary Layer on Cone in Supersonic Flow at Large Angle of Attack," TN L844, Nov. 1952, NACA.

[13] Richtmyer, R. D. and Morton, K. W., *Difference Methods for Initial Value Problems*, Interscience, New York, 1967.